energies

MDPI

Article

Application of the Feedback Linearization in Maximum Power Point Tracking Control for Hydraulic Wind Turbine

Chao Ai [1,2], Wei Gao [1,2], Qinyu Hu [1,2], Yankang Zhang [3], Lijuan Chen [3,*], Jiawei Guo [1,2] and Zengrui Han [1,2]

1 Hebei Heavy Machinery Fluid Power Transmission and Control Laboratory, Yanshan University, Qinhuangdao 066004, China; aichao@ysu.edu.cn (C.A.); gaowei2018@njit.edu.cn (W.G.); huqingyu@stumail.ysu.edu.cn (Q.H.); 708951592@stumail.ysu.edu.cn (J.G.); hzr@stumail.ysu.edu.cn (Z.H.)
2 School of Mechanical Engineering, Yanshan University, Qinhuangdao 066004, China
3 Nanjing Institute of Technology, Nanjing 211167, China; zhangyk@njit.edu.cn
* Correspondence: chenlj@njit.edu.cn; Tel.: +86-18713508769

Received: 11 February 2020; Accepted: 17 March 2020; Published: 24 March 2020

Abstract: Taking the hydraulic wind turbine as the research object, the method is studied to improve the utilization ratio of wind energy for hydraulic wind turbine, when the wind speed is lower than the rated wind speed. The hydraulic fixed displacement pump speed and generating power can be used as control output to realize the maximum power point tracking control. The characteristics of the maximum power point tracking control are analyzed for hydraulic wind turbine, and the hydraulic output power is taken as control output based on the comprehensive performance requirements. Because the hydraulic wind turbine is a strong multiplication nonlinear system, the system is globally linearized based the feedback linearization method, and the maximum power point tracking control law is obtained. The simulation and experiment results show that the system has good dynamic performance with the proposed control law. The control provides theoretical guidance for optimal power tracking control law application for hydraulic wind turbine.

Keywords: hydraulic wind turbine; maximum power point tracking control; hydraulic fixed displacement pump; hydraulic variable displacement motor; feedback linearization method

1. Introduction

Wind energy is a vast renewable energy resource being increasingly tapped by wind turbines which are growing in number and size. Conventional wind turbines transmissions consist of a mechanical gearbox and high-speed generator, or sometimes direct drive low-speed generators are used as described in [1]. But these two traditional transmission schemes have some disadvantages, such as high cost and high failure rate. In order to reduce the cost and improve the reliability, hydrostatic transmission has been proposed in [2–4]. Thus, the power captured by the turbine rotor will be transmitted to the generator through the hydrostatic transmission, and the generator can be flexibly installed, either in the nacelle of the wind turbine or installed on the ground driven by hydraulic pipelines, which greatly reduces the difficulty of installation and maintenance. Benefits of the hydraulic wind turbine (HWT) are that the hydrostatic transmission is inherently more compliant than the mechanical transmission, which makes it more reliable in face of shock loading, and the transmission ratio is adjustable, so the system does not need additional frequency conversion devices to coordinate wind turbine speed and power grid frequency. Meanwhile, with the development of digital hydraulic technology, the low part-load efficiency of conventional hydraulics is solved [5].

In order to improve the efficiency of wind energy utilization, scholars at home and abroad have done a lot of research on the maximum power point tracking (MPPT) control for HWT. An optimal H∞ ring forming pressure controller was designed for a mechano-hydraulic hybrid wind turbine, which can accurately track the optimal load pressure in [6]. The small signal linearization and variable gain proportional integral differentiation (PID) were combined to solve the problem of inconsistent power response, and the speed control loop is used to optimize the MPPT strategy in [7]. A sensorless double integral sliding mode controller was designed to achieve maximum power extraction under the condition of large parameter uncertainty and nonlinearity for hydrostatic tidal turbine in [8]. A PID controller and a sliding mode controller were applied for speed control to track a predefined speed in [9]. To track the maximum power point, a takagi-sugeno (TS) fuzzy model was proposed for the HWT with two variable displacement pumps and a fixed displacement motor, and a parameter varying model predictive control (PVMPC) approach was designed in [10]. Shengquan Li proposed a combined model predictive control strategy to achieve the purpose of MPPT control for HWT in [11]. SP Mulders proposed an implementation, model-free, gradient-based and extremum seeking control optimization strategy to achieve an average maximum power increase in [12]. M, Deldar designed a decentralized control configuration to collect the maximum energy without directly measuring the wind speed in [13]. A digital hydrostatic drive solution was introduced in the HWT to largely utilize the energy captured by the rotor in [14], and the kW^2 control law combined with digital hydrostatic method was proposed to improve HWT energy production. Active disturbance rejection controller (ADRC) control method was introduced to achieve HWT MPPT control, and the pump speed was taken as the control output in [15]. However, the MPPT control smoothness needed to be further improved. The frequency control and the MPPT control rely on the mechanical torque adjustment on the hydraulic motor that was coupled with the generator in [16]. A MPPT control strategy based on the tip speed ratio (TSR) was adopted for the 600 kW hydraulic energy storage wind turbine, and the maximum power tracking performance was simulated and analyzed by subjecting to turbulent speed condition in [17].

The above-mentioned researches on MPPT control methods verify the proposed controller effectiveness from a theoretical point view and provide a certain reference. However, according to the HWT with a fixed displacement pump and a variable displacement motor, it is also necessary to explore a MPPT controller. Therefore, based on the HWT working principle, a state space model is established. Because the hydraulic main transmission system has strong nonlinearity, wind has randomness and volatility, and sometimes the fluctuation range is large, the feedback linearization method can rid the system of small signal linearization limitation, and the analysis and synthesis of the system in a large range is realized [18]. Thus, the feedback linearization method is adopted to conduct the MPPT controller.

The paper is organized as follows: the HWT working principle and the requirements for MPPT control are introduced in Section 2. The HWT mathematical model is established in Section 3. In Section 4, the feedback linearization method is used to globally linearize the system, and the MPPT controller is proposed with the output of power. In Section 5, the simulation results are carried out under the different conditions, and the experiment results are also carried out based on the 24 kW HWT experiment platform. Finally, conclusions are drawn in Section 6.

2. Description of the HWT

2.1. HWT Working Principle

HWT is mainly composed of a rotor, a fixed displacement pump, a variable displacement motor and a synchronous generator. An inverter for frequency conversion is not required. The rotor and the pump are coaxially connected, and the pump supplies high pressure oil to the motor, so the fluctuation of the wind speed tends to affect the motor speed [19,20]. The motor and the generator are also coaxially connected, and the motor and generator speed are controlled by changing the motor displacement. When the synchronous generator is stable within the required speed range (1500 r/min ± 6 r/min), it can be connected to the grid for power generation. At the same time, the charge pump provides hydraulic oil for the low-pressure pipeline, the control pump provides hydraulic oil for control pipeline of the variable displacement motor, and the safety relief valve and relief valve are used for system protection. A schematic diagram of the HWT is shown in Figure 1.

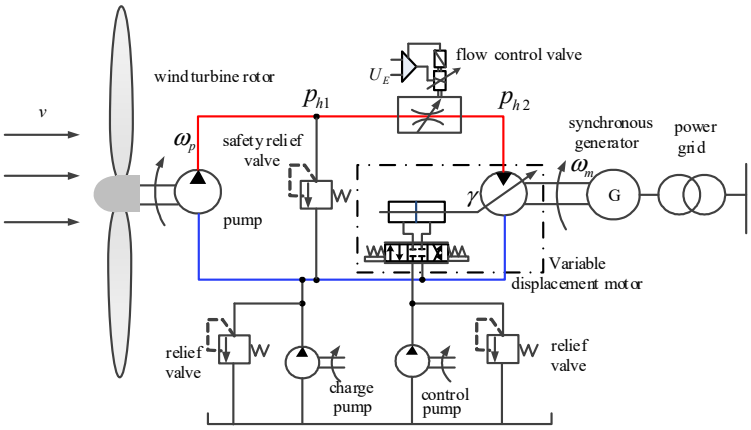

Figure 1. Schematic of the hydraulic wind turbine (HWT).

2.2. Control Effects of MPPT

The maximum wind power captured by the wind turbine under the demand wind speed [21] is expressed as

$$P_{\mathrm{rmax}} = \frac{1}{2}\rho\pi R^2 v^3 C_{p\max} \tag{1}$$

The rotor speed is related to the wind speed, and the rotor speed is expressed as

$$\omega = \frac{v\lambda_{opt}}{R} \tag{2}$$

From the Equations (1) and (2), the relationship between the captured maximum wind power and the rotor speed (the pump speed) can be expressed as

$$\mathrm{P}_{r\max} = \frac{\rho\pi R^5 C_{p\max}}{2\lambda_{opt}^3}\omega^3 = K_P\omega^3 \tag{3}$$

The principle of the MPPT method for direct generation power control is shown in Figure 2, and the tracking process is expressed as follows:

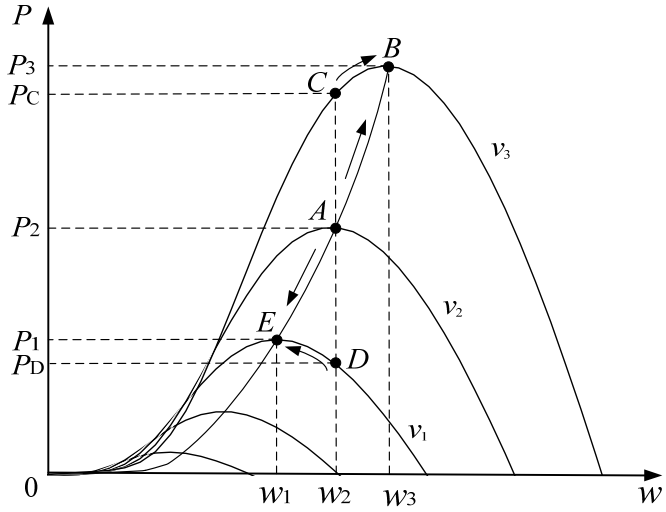

Figure 2. Schematic of the maximum power point tracking (MPPT) method for direct generation power control.

Assuming wind speed $v_1 < v_2 < v_3$, E, A, and B are the maximum power points at the three kinds of wind speed, respectively. The initial wind speed is v_2, and initially the wind turbine works stably at point A, which is the maximum power point at wind speed v_2.

When the wind speed increases from v_2 to v_3, since the rotor speed cannot change suddenly, the input power is the power P_C corresponding to point C, and the power value is the power P_2 corresponding to point A. Since the input power P_C is always greater than the generating power P_2 before point B, the rotor will accelerate. As the rotor speed increases, the input power moves from point C to the maximum power point B along the power characteristic curve of v_3; the actual generating power moves from point A to point B along the demand value of the generating power (the optimal power curve). The rotor input power is equal to the demand power at point B, and the system is re-balanced. At this point, the MPPT process is completed when the wind speed increases from v_2 to v_3.

In a similar way, when the wind speed decrease from v_2 to v_1, since the rotor speed cannot change suddenly; the input power is the power P_D corresponding to point D, and the power value is the power P_2 corresponding to point A. Since the input power P_D is always less than the generating power P_2 before point E, the rotor will slow down. As the rotor speed decreases, the input power moves from point D to the optimal power point E along the power characteristic curve of v_1. The actual generating power moves from point A to point E along the demand value of the generating power (the optimal power curve). The input power is equal to the demand value of power generation at point E, and the system is re-balanced. At this point, the MPPT process is completed when the wind speed decreases from v_2 to v_1.

Based on the above principle analysis, the MPPT method of direct generation power control can automatically track the wind turbine to the maximum power point. The rapidity and accuracy of the MPPT process is taken into account.

3. The Mathematical Model of the Hydraustatic Transmission

3.1. The Pump Model

The pump shaft torque is related to the pressure, and the torque is expressed as

$$T_p = \frac{D_p p_{h1}}{\eta_{mech,p}} \tag{4}$$

The difference between the rotor and pump torque accelerates the combined inertia and overcomes viscous friction. The torque balance equation is expressed as

$$T_v\left(\omega_p, v\right) - T_p = J_p \frac{\mathrm{d}\omega_p}{\mathrm{d}t} + B_p \omega_p \tag{5}$$

Flow continuity equation of the fixed displacement pump is expressed as

$$Q_p = D_p \omega_p - C_{t1} p_{h1} \tag{6}$$

From the Equations (4)–(6), the state equation of the pump speed can be expressed as

$$\dot{\omega}_p = \frac{1}{J_p}\left(T_r - \frac{D_p p_{h1}}{\eta_{mech,p}} - B_p \omega_p\right) \tag{7}$$

3.2. The Motor Model

Similarly, the motor output torque is related to pressure, and the torque is expressed as

$$T_m = D_m p_{h2} \eta_{mech,m} = K_m \gamma p_{h2} \eta_{mech,m} \tag{8}$$

The difference between the motor and generator torque accelerates the motor inertia and overcomes the viscous friction. The torque balance equation is expressed as

$$T_m - T_L = J_m \frac{\mathrm{d}\omega_m}{\mathrm{d}t} + B_m \omega_m \tag{9}$$

And the variable motor flow continuity equation is expressed as

$$Q_m = D_m \omega_m + C_{t2} p_{h2} \tag{10}$$

From the Equations (8)–(10), the state equation of the motor speed is

$$\dot{\omega}_m = \frac{1}{J_m}\left(K_m \gamma p_{h2} \eta_{mech,m} - B_m \omega_m - T_L\right) \tag{11}$$

3.3. The Flow Control Valve Model

The flow through the proportional flow control valve is expressed as

$$Q_{bl} = K U_E \tag{12}$$

3.4. The Hose Model

The oil flows between pump and motor inside a hose, and the general equation for the additional flow caused by oil compressibility and hose compliance is expressed as

$$Q_c = \frac{V}{\beta_e} \frac{\mathrm{d}p_h}{\mathrm{d}t} \tag{13}$$

The proportional flow control valve divides the high-pressure line into two parts, one is the pump to the flow control valve, with volume V_1, and the other part is the flow control valve to the motor, with volume V_2.

3.5. The Hydraulic Transmission System State Space Model

The compressibility flow between the pump and the flow control valve is expressed as

$$Q_{c1} = Q_p - Q_{bl} = D_p\omega_p - C_{t1}p_{h1} - KU_E \tag{14}$$

The compressibility flow between the flow control valve and the motor is expressed as

$$Q_{c2} = Q_{bl} - Q_m = KU_E - D_m\omega_m - C_{t2}p_{h2} \tag{15}$$

To establish the state space model of the main transmission system for the HWT, the following assumptions need to be made:

(1) The pressure in the low-pressure line is a constant.
(2) The leakage coefficient, the viscous damping coefficient and the bulk modulus of the oil are the fixed values, which do not change with temperature or other factors.
(3) The pressure loss in the hydraulic lines is ignored.
(4) The pump mechanical efficiency $\eta_{\mathrm{mech,p}}$ is designed 1.

The system state space model is obtained by combining the Equations (7), (11)–(15).

$$\begin{cases} \dot{\omega}_p = -\frac{B_p}{J_p}\omega_p - \frac{D_p}{J_p}p_{h1} + \frac{1}{J_p}T_v\left(\omega_p, v\right) \\ \dot{p}_{h1} = \frac{D_p\beta}{V_1}\omega_p - \frac{C_{t1}\beta}{V_1}p_{h1} - \frac{K\beta U_E}{V_1} \\ \dot{p}_{h2} = \frac{K\beta U_E}{V_2} - \frac{C_{t2}\beta}{V_2}p_{h2} - \frac{K_m\beta\omega_m}{V_2}\gamma \\ \dot{\omega}_m = -\frac{B_m}{J_m}\omega_m + \frac{K_m p_{h2}}{J_m}\gamma - \frac{1}{J_m}T_L \end{cases} \tag{16}$$

Due to the MPPT control process, the grid-connected speed control has been completed, and the motor speed is constant; that is, $\omega_m = 1500\mathrm{r/min}$. Moreover, the proportional throttle valve opening is open. Thus, the system status values are the pump speed and the pressure between the pump and variable displacement motor. The state equation during power tracking can be expressed as

$$\begin{cases} \dot{\omega}_{\mathrm{p}} = -\frac{B_{\mathrm{p}}}{J_{\mathrm{p}}}\omega_{\mathrm{p}} - \frac{D_{\mathrm{p}}}{J_{\mathrm{p}}}p_{\mathrm{h}} + \frac{1}{J_{\mathrm{p}}}T_{\mathrm{r}}\left(\omega_{\mathrm{p}}, v\right) \\ \dot{p}_{\mathrm{h}} = \frac{D_{\mathrm{p}}\beta}{V}\omega_{\mathrm{p}} - \frac{C_{\mathrm{t}}\beta}{V}p_{\mathrm{h}} - \frac{K_{\mathrm{m}}\omega_{\mathrm{md}}\beta}{V}\gamma \end{cases} \tag{17}$$

The state variables is define as $x_1 = \omega_{\mathrm{p}}$, $x_2 = p_{\mathrm{h}}$, and the system control input is $u = \gamma$. Therefore, the system state space model after grid-connection can be expressed as

$$\begin{cases} \dot{x}_1 = -\frac{B_{\mathrm{p}}}{J_{\mathrm{p}}}x_1 - \frac{D_{\mathrm{p}}}{J_{\mathrm{p}}}x_2 + \frac{1}{J_{\mathrm{p}}}T_{\mathrm{r}}(x_1, v) \\ \dot{x}_2 = \frac{D_{\mathrm{p}}\beta}{V}x_1 - \frac{C_{\mathrm{t}}\beta}{V}x_2 - \frac{K_{\mathrm{m}}\omega_{\mathrm{md}}\beta}{V}u \end{cases} \tag{18}$$

The system model is rewritten into affine nonlinear form $\dot{\boldsymbol{x}} = \boldsymbol{f}(\boldsymbol{x}) + \boldsymbol{g}(\boldsymbol{x})u$, the system state space model after grid grid-connection can be expressed as

$$\boldsymbol{f}(\boldsymbol{x}) = \begin{bmatrix} -\frac{B_p}{J_{\mathrm{p}}} & -\frac{D_{\mathrm{p}}}{J_{\mathrm{p}}} & \frac{1}{J_{\mathrm{p}}} \\ \frac{D_{\mathrm{p}}\beta}{V} & -\frac{C_{\mathrm{t}}\beta}{V} & 0 \end{bmatrix} \begin{bmatrix} x_1 \\ x_2 \\ T_{\mathrm{r}}(x_1, v) \end{bmatrix} \tag{19}$$

$$g(x) = \begin{bmatrix} 0 \\ -\frac{K_{\mathrm{m}}\omega_{\mathrm{md}}\beta}{V} \end{bmatrix} \tag{20}$$

4. The MPPT Controller Based on Feedback Linearization Method

4.1. Control Thoughts

In the MPPT method for direct power generation control, the control system mainly includes three control loops, which are the motor displacement reference control loop, the motor speed control loop, and the power control loop. Among the three control loops, the motor displacement reference control loop is calculated from the fixed displacement pump speed based on the traffic conservation, and the purpose of the motor displacement reference control loop is to make the variable motor work at the excitation synchronous speed. The motor speed control loop is the motor displacement fine-tuning amount, formed by the deviation between the demand synchronous speed (1500 r/min) and the actual motor speed. The function of the motor speed control loop is to control the variable motor to work precisely at the synchronous speed and achieve quasi-synchronous grid connection. Power control loop is the reference value of the maximum power, which is calculated by the actual pump speed according to the optimum blade tip ratio and the maximum wind energy utilization coefficient. Compared with the actual power, the deviation is formed, and the displacement compensation value is adjusted by the controller. The specific control block diagram is shown in Figure 3.

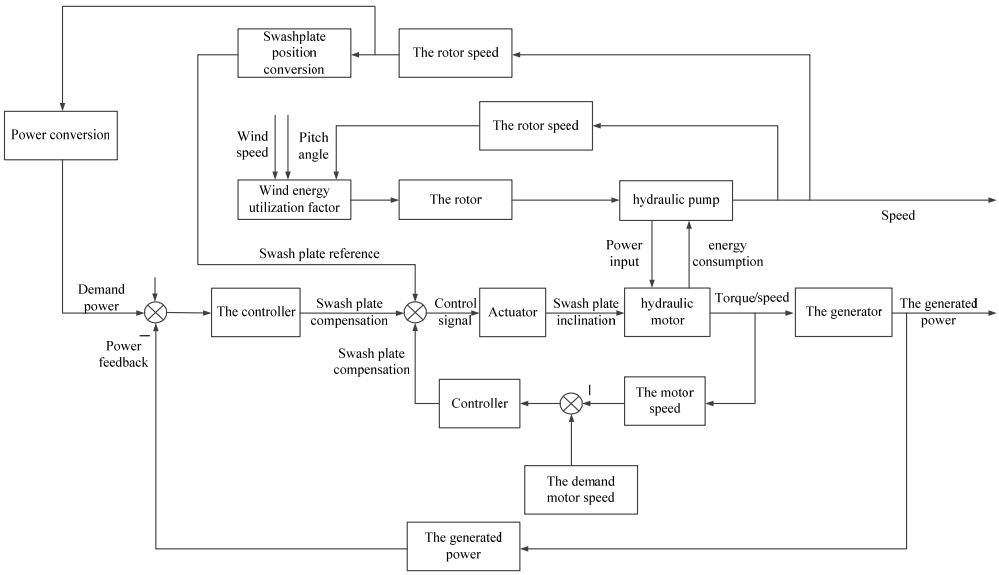

Figure 3. HWT MPPT control block diagram.

4.2. MPPT Controller Design

The process of solving the system control law using the feedback linearization method is shown in Figure 4 [18–22].

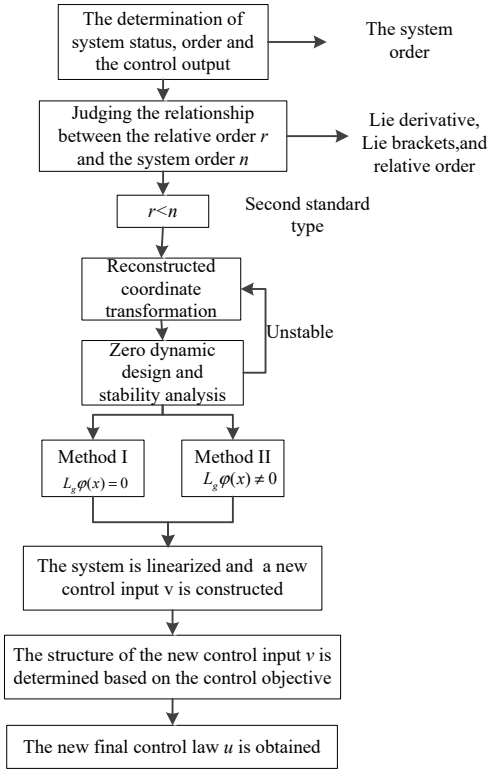

Figure 4. Feedback linearization control law flowchart.

4.2.1. Control Output

The control output is expressed as

$$y = h(x) = D_{\mathrm{p}} x_1 x_2 = D_{\mathrm{p}} \omega_{\mathrm{p}} p_{\mathrm{h}} \tag{21}$$

4.2.2. Relative Order

The definition of relative order is as follows: (1) The Lie derivative value of the k-order Lie derivative of the output function $h(x)$ to the vector field $\boldsymbol{F}(\boldsymbol{x})$ to the vector field $\boldsymbol{F}(\boldsymbol{x})$ in the neighborhood of $x = x_0$ is zero; that is, $L_g L_f^k h(x) = 0$. (2) The Lie derivative value of the $(r-1)$-order Lie derivative $(k < r-1)$ of the output function $h(x)$ to the vector field $\boldsymbol{F}(\boldsymbol{x})$ to the vector field $\boldsymbol{F}(\boldsymbol{x})$ in the neighborhood of $x = x_0$ is not zero; that is, $L_g L_f^{r-1} h(x) \neq 0$. Then the relative degree of nonlinear system (18) in $x = x_0$ is defined as r [18–22].

From the equations (17)–(20), according the relevant definition of the Lie derivative, the relative order evaluation expression is

$$L_{\mathrm{g}} L_{\mathrm{f}}^0 h(x) = -\frac{K_{\mathrm{m}} \beta \omega_{\mathrm{md}} D_{\mathrm{p}} x_1}{V} \neq 0 \tag{22}$$

From the expression (22), the relative order $r = 1 < 2$, the system cannot be linearized in full state and zero dynamic design is required.

From the above analysis, the system cannot be completely linearized. Therefore, input–output linearization and the zero dynamic design method are adopted to determine the system controller [22].

In the process of zero dynamic design, the system dynamic behavior can be divided into the external dynamics and internal dynamics. The external dynamics are not only required to be stable but also have tracking performance and reject disturbance. The internal dynamics are only required to be stable.

4.2.3. Zero Dynamic Controller Design

The zero dynamics selected in this paper is $\varphi_2(x) = x_1$, the pump speed, which is considered as the internal dynamics. First, a coordinate transformation of the system gives

$$\begin{cases} z_1 = \varphi_1(\boldsymbol{x}) = h(\boldsymbol{x}) = D_p x_1 x_2 \\ z_2 = \eta_2(\boldsymbol{x}) = x_1 \end{cases} \tag{23}$$

Thus, the Jacobian matrix of the vector function $\varphi(x) = [z_1(x)\ z_2(x)]^{\mathrm{T}}$ at $x = x_0$ is expressed as

$$J_\varphi = \frac{\partial \phi(x)}{\partial(x)}\Big|_{x=x_0} = \begin{bmatrix} D_{\mathrm{p}} x_2 & D_{\mathrm{p}} x_1 \\ 1 & 0 \end{bmatrix} \tag{24}$$

This is a non-singular at $\boldsymbol{x} = \boldsymbol{x}_0$, so the coordinate transformation is valid.

And then the inverse mapping of $z = \varphi(x)$ is $x = \varphi^{-1}(z)$. Therefore, the x can be expressed as

$$\begin{cases} x_1 = z_2 \\ x_2 = \frac{z_1}{D_p z_2} \end{cases} \tag{25}$$

From the equations (18) and (25), the final expression of the system in $\boldsymbol{z}$ coordinates can be expressed as

$$\begin{cases} \dot{z}_1 = D_{\mathrm{p}} \frac{z_1}{D_{\mathrm{p}} z_2}\left(-\frac{B_{\mathrm{p}}}{J_{\mathrm{p}}} z_2 - \frac{D_{\mathrm{p}}}{J_{\mathrm{p}}} \frac{z_1}{D_{\mathrm{p}} z_2} + \frac{1}{J_{\mathrm{p}}} T_{\mathrm{r}}(z_2, v)\right) + D_{\mathrm{p}} z_2 \left(\frac{D_{\mathrm{p}} \beta}{V} z_2 - \frac{C_{\mathrm{t}} \beta}{V} \frac{z_1}{D_{\mathrm{p}} z_2}\right) u \\ \dot{z}_2 = -\frac{B_{\mathrm{p}}}{J_{\mathrm{p}}} z_2 - \frac{1}{J_{\mathrm{p}}} \frac{z_1}{z_2} + \frac{1}{J_{\mathrm{p}}} T_{\mathrm{r}}(z_2, v) \end{cases} \tag{26}$$

The system output in the $\boldsymbol{z}$ coordinate system is expressed as

$$y = z_1 \tag{27}$$

The external state, which is the pump outlet power, is close to zero and in a stable state, that is, $z_1 = 0, \dot{z}_1 = 0$. At this point, the equations (26) can be expressed as

$$\dot{z}_2 = -\frac{B_{\mathrm{p}}}{J_{\mathrm{p}}} z_2 + \frac{1}{J_{\mathrm{p}}} T_{\mathrm{r}}(z_2, v) \tag{28}$$

When the external state is close to zero, the internal state stability is related to the pump external load, and it is irrelevant to u, but all are asymptotically stable. Therefore, the system has zero dynamic stability and can be solved by the controller [23].

After the coordinate transformation and the zero-dynamic design, the HWT MPPT controller can be designed based on the feedback linearization control method. The specific method is to linearize the system in the coordinate system, and the output and the control input of the system are linearly related.

First, the desired control input is constructed as $\dot{z}_1 = v^*$. At this point, the system output and the constructed input v^* are linearly dependent. The constructed input is expressed as

$$v^* = D_{\mathrm{p}} x_2 \left(-\frac{B_{\mathrm{p}}}{J_{\mathrm{p}}} x_1 - \frac{D_{\mathrm{p}}}{J_{\mathrm{p}}} x_2 + \frac{1}{J_{\mathrm{p}}} T_{\mathrm{r}}(x_1, v)\right) + D_{\mathrm{p}} x_1 \left(\frac{D_{\mathrm{p}} \beta}{V} x_1 - \frac{C_{\mathrm{t}} \beta}{V} x_2\right) u \tag{29}$$

Then the system can be linearized as follows:

$$\begin{cases} \dot{z}_1 = v^* \\ \dot{z}_2 = -\frac{B_p}{J_p} z_2 - \frac{1}{J_p} \frac{z_1}{z_2} + \frac{1}{J_p} T_v(z_2, v) \end{cases} \tag{30}$$

Thus, the zero dynamics is asymptotically stable, and the whole system is asymptotically stable. That is, the selected coordinate transformation can be used to solve the controller, and the system is in a stable state under the controller.

Thus, the motor control input can be expressed in terms of v^*

$$u = -\frac{V}{K_m\beta\omega_{md}D_px_1}\left(v - \left[D_px_2\left(-\frac{B_\mathrm{p}}{J_p}x_1 - \frac{D_p}{J_p}x_2 + \frac{1}{J_p}T_v(x_1, v^*)\right) + D_px_1\left(\frac{D_p\beta}{V}x_1 - \frac{C_t\beta}{V}x_2\right)\right]\right) \tag{31}$$

4.2.4. Output Reference Design

When the power is taken as control output, the demand maximum power at each wind speed is expressed as

$$y_\mathrm{d} = K_\mathrm{p}\omega_\mathrm{p}^3 = \frac{\rho\pi R^5 C_\mathrm{pmax}}{2\lambda_\mathrm{opt}^3}\omega_\mathrm{p}^3 \tag{32}$$

4.2.5. Controller Design

In the control process of the MPPT, theoretically, the system is linearized precisely. However, there will be tracking errors due to model parameters. The closed loop PI control is used to reduce the tracking error.

The tracking error is defined as

$$e = y_\mathrm{d} - y \tag{33}$$

and the new control input [24] is expressed as

$$v^* = \dot{y}_\mathrm{d} + k_1 e + k_2\int e dt \tag{34}$$

In (34), the values of k_1, k_2 are turned according to the control requirements.

The final controller is given by (31) and (34). The controller expressed in terms of physical variables is:

$$\gamma = \frac{D_p\omega_p - C_tp_h}{K_m\omega_{md}} - \frac{V}{K_m\beta\omega_{md}D_p\omega_p}(v^* - D_pp_h\dot{\omega}_p) \tag{35}$$

According to the (35), the system states and constructed control inputs are combined linearly to form the control signal for the motor displacement. Through the real-time detection of system states, the calculated control signals are sent to the system to realize the MPPT control.

Comprehensively considering the rapidity, accuracy and stability of the power tracking of the hydraulic wind turbine and combining the effects of the proportional and integral links on the control system, the control parameters are shown in Table 1.

Table 1. Control parameters.

Number	Parameter Symbol	Value
1	k_1	6
2	k_2	4

5. Simulation and Experiment Research

5.1. Simulation Platform

A mathematical model, as showed in Figure 5., is established in MATLAB/Simulink® software. The nonlinear controller accuracy, which is based on the feedback linearization theory, can be verified under different kinds of wind speed. The corresponding parameters of the system are shown in Table 2.

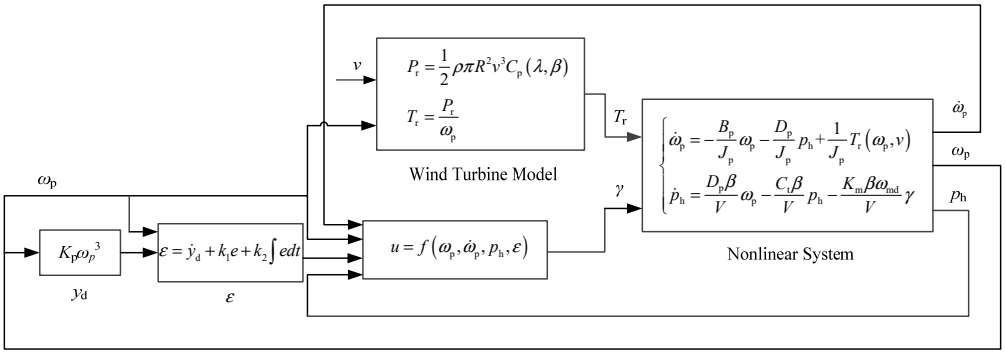

Figure 5. Simulation model.

Table 2. Parameters of hydraulic drive system for experimental platform.

Parameter Symbol	Parameter Name	Value	Unit
B_p	the viscous damping coefficient of hydraulic pump	0.4	N.m.s/rad
D_p	the displacement of hydraulic pump	1×10^{-5}	m^3/rad
J_p	the inertia of hydraulic pump	400	kg/m^3
K_m	the displacement gradient of variable displacement motor	5.366×10^{-6}	m^3/rad
B_m	the viscous damping coefficient of variable displacement motor	0.0345	N.m.s/rad
J_m	the inertia of hydraulic motor	0.462	kg/m^3
β_e	the bulk modulus of hydraulic oil	743×10^6	Pa
C_t	the total leakage coefficient of hydraulic pump and variable displacement motor	6.28×10^{-12}	m^3/(s.Pa)
V	the volume of oil affected by pressure effect in hydraulic hose	2.8×10^{-3}	m^3
P	the output power of wind turbine	24	kW
R	radius of wind turbine	7.48	m
C_{pmax}	the maximum coefficient of wind energy utilized	0.4496	
λ_{max}	the optimal tip speed ratio	22.77	

5.2. Simulation Analysis

In order to verify the proposed control method effectiveness, the HWT MPPT control are researched based on the above simulation platform. Under the condition of 7 m/s–8 m/s step wind speed at 10 s, the response characteristics of system are observed during the process of the power tracking, and the specific curves are shown in Figure 6.

Under the condition of 8 m/s–7 m/s step wind speed at 10 s, the response characteristics of system are observed during the process of the power tracking, and the specific curves are shown in Figure 7.

From the results of Figure 6; Figure 7, the pump speed and high pressure change with the step wind speed, and the demand power curve coincides with the output power curve; that is, the output power can track the demand power. The MPPT controller effectiveness is verified. There is a difference between the input wind power and output power, and the difference is 1 kW; the reason is that in the pump–motor system there is transmission efficiency.

There are two main types of energy loss in the process of energy flow conversion, which are the energy lost by the hydraulic transmission system and the energy lost by the generator. Among them, the energy lost by the hydraulic transmission system mainly includes volume loss and oil heating loss, and the energy lost by the generator mainly includes mechanical loss and electromagnetic loss. The wind energy absorbed by the wind turbine cannot be completely converted into electrical energy with these unavoidable energy losses.

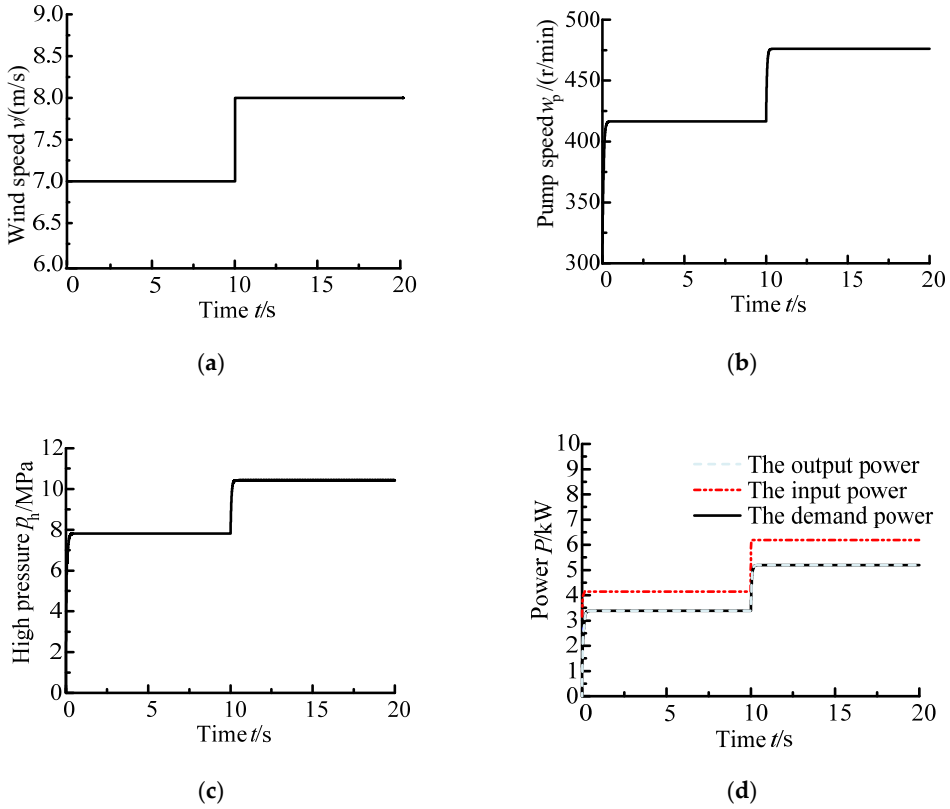

Figure 6. The response curve under the condition of 7 m/s-8 m/s step wind speed at 10 s. (**a**) the wind speed; (**b**) the pump speed; (**c**) the high pressure; (**d**) the output power.

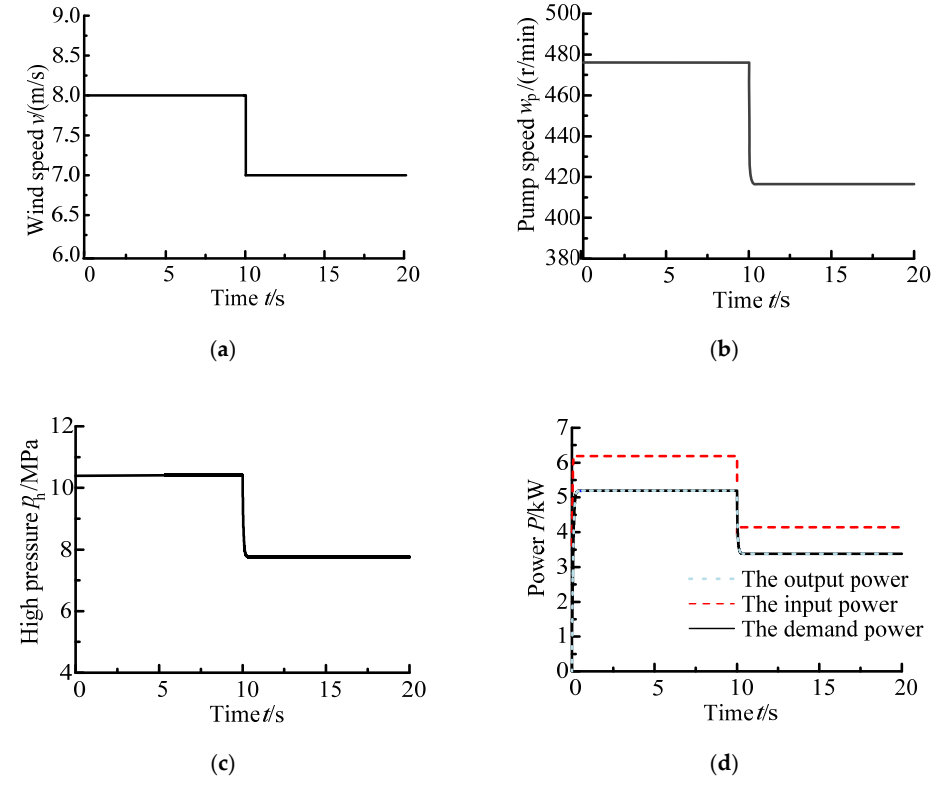

Figure 7. the response curve under the condition of 8 m/s-7 m/s step wind speed at 10 s. (**a**) the wind speed; (**b**) the pump speed; (**c**) the high pressure; (**d**) the output power.

Under the conditions of 7 m/s (± 0.5 m/s)–8 m/s (± 0.5 m/s) in wind speed, the response characteristics of system are observed during the process of the power tracking, and the specific curves are shown in Figure 8.

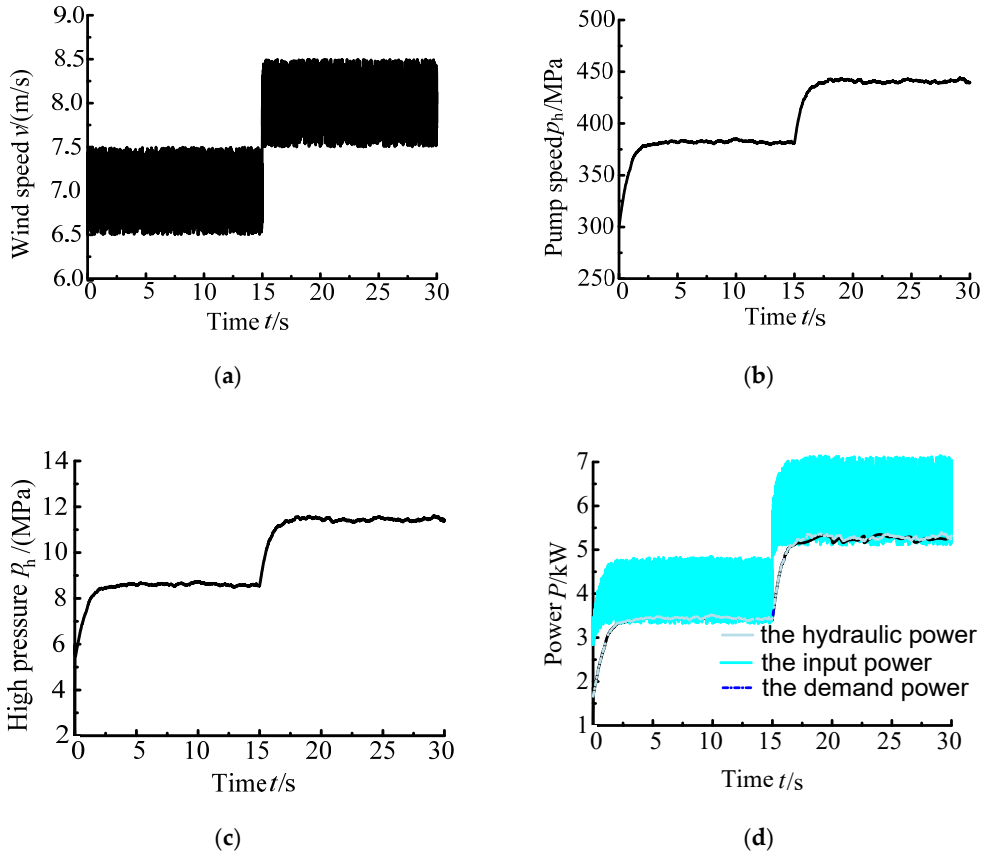

Figure 8. The response curve under 8 ± 0.5 m/s wind speed. (**a**) the wind speed; (**b**) the pump speed; (**c**) the high pressure; (**d**) the output power.

From the results of Figure 8, the pump speed and high pressure also change with the fluctuated speed, and the demand power curve also coincides with the output power curve; that is, the output power can track the demand power. The motor swing angle is adjusted to achieve the above results, and the MPPT controller effectiveness is verified further. There is a difference between the input wind power and output power; the difference is 1.2 kW, and the reason is that in the pump–motor system there is transmission efficiency.

5.3. Experiment Platform

The 24 kW HWT experiment simulation platform is shown in Figure 9. The system major hardware models are shown in Table 3. The experimental platform mainly consists of four parts: wind turbine simulation system, hydraulic transmission system, grid-connected generation system and control system. Among them, the frequency converter is used to control the frequency conversion motor to simulate the wind turbine.

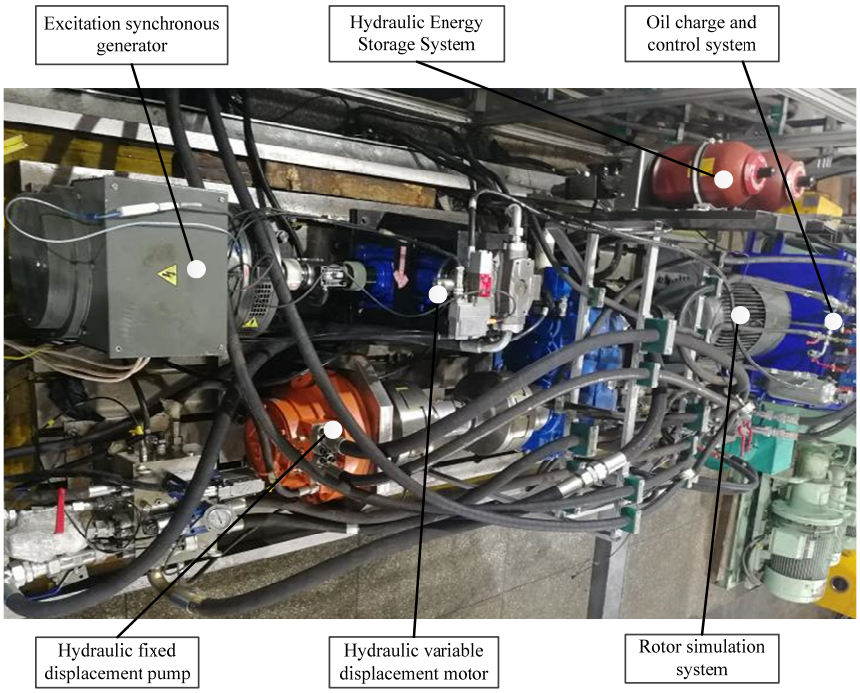

Figure 9. The structure diagram of 30 kVA semi-physical simulation platform.

Table 3. 24 kW semi physical simulation experiment platform components.

Serial Number	Name	Model
1	variable frequency motor	yvp250m-4
2	speed torque sensor	jn338a
3	hydraulic fixed displacement pump	a2f63r2p3
4	pressure sensor	zq-bz-1/hk/m20
5	pressure gauge	yn-63-i-31.5
6	relief valve	db10a-1-b30/315
7	check valve	s20p1.0b
8	accumulator	sb330-10a1/112a9-330a
9	variable displacement motor	a4vso40ds1/10w-ppb13t013z
10	excitation synchronous generator	wf200-24
11	vane pump	pfe-41085
12	relief valve	agm20-a-20/100y
13	relief valve	agm20-a-20/315y
14	constant pressure variable pump	63pcy14-1b
15	relief valve	dbds10g10b/25/2
16	air cooler	ok-el5s/3.1/m/a/1

5.4. Experiment Analysis

Based on the above experimental platform and the pre-determined parameters, the MPPT control effect are researched under step wind speed of 8 m/s–9 m/s at 8 s, and the wind speed, the pump speed, system power, and high pressure are shown in Figure 10.

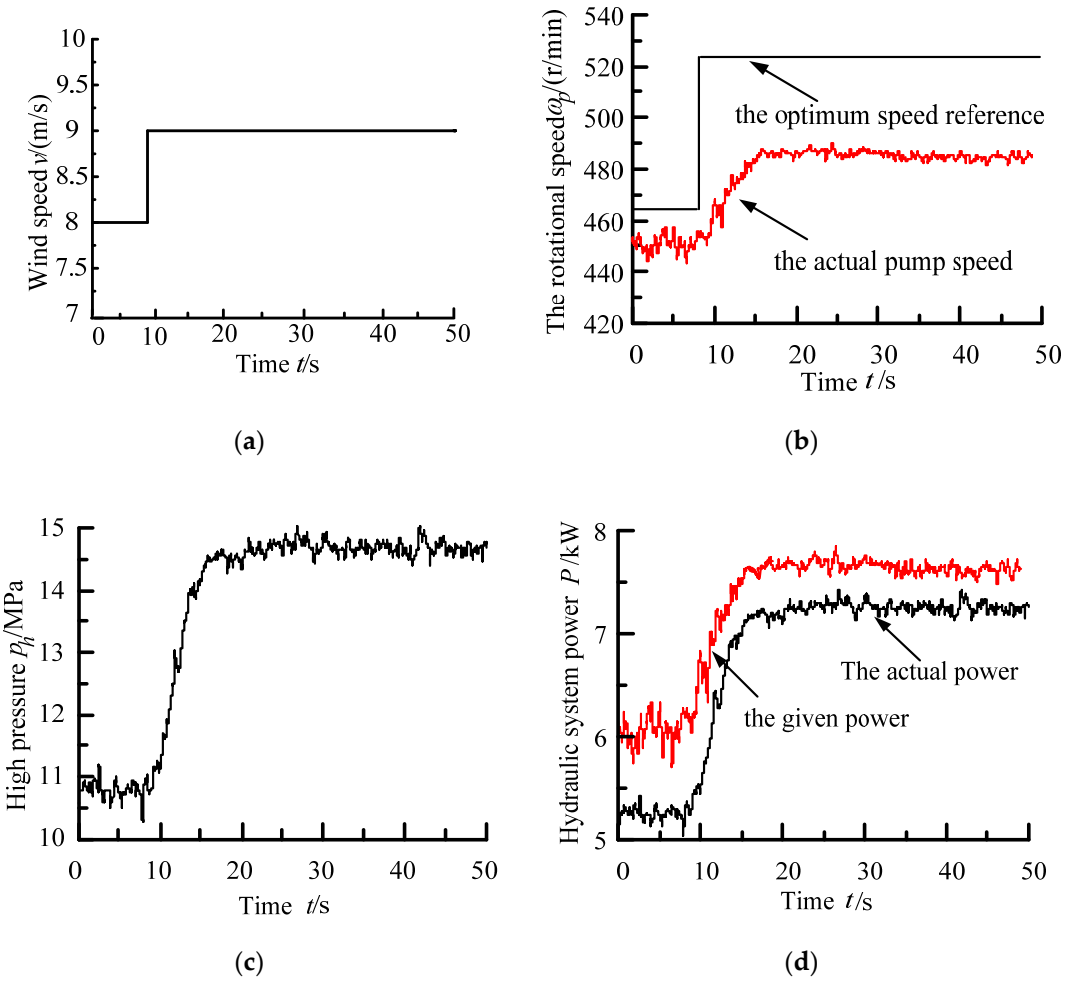

Figure 10. The system response curve under the step wind speed. (**a**) the wind speed; (**b**) the pump speed; (**c**) the high pressure; (**d**) the output power.

From Figure 10, through adjusting the motor displacement, the high pressure and pump speed change with step wind speed, the actual power also changes with the demand power. The response characteristics are basically the same as the simulation, and the system state changes stably under the step wind speed. However, there are differences between the demand power and actual power, and the reason is that the MPPT controller accuracy depends on the parameters.

The experimental parameters can be re-determined by experimental data. V/β can be obtained by the above experimental data. When the system is in a stable state, the dynamic change is equal to zero. Therefore, the acceleration term in the controller is 0, and the calculating formula for the motor swing angle can be expressed as

$$\gamma = \frac{D_p\omega_p - C_t p_h}{K_m\omega_{md}} - \frac{V}{\beta}\frac{k_1\Delta P}{K_m\omega_{md}D_p\omega_p} \tag{36}$$

where $v = \mathrm{d}\left(D_p\omega_p p_h\right)/\mathrm{d}t$.

According to Formula (36), the controller contains three items, including the pump input flow, the leakage caused by the pressure and the oil-hydraulic contraction caused by the pressure. The first two items are the steady-state term, and the oil-hydraulic contraction caused by the pressure is the dynamic adjustment term. The HWT MPPT controller essentially converts power deviation into pressure change rate to dynamically adjust the motor displacement. The final steady-state term has a great influence on the system control. When the system reaches a stable state, the motor displacement should be the

corresponding steady-state value related to the pump speed and the high pressure so that different power can be generated under each stable pump speed. Otherwise, repeated dynamic adjustments are needed to achieve stability. The pump displacement is a constant, so the leakage coefficient at different pump speed will ultimately affect the system stability. If the steady value is not accurate, it is easy to cause power generation instability by adjusting the dynamic term. Instead, the system will stabilize in other states. Therefore, it is difficult to guarantee the control accuracy in practical application, but the controller provides theoretical direction.

6. Conclusions

This paper takes the HWT as the research object; the state space model is established for HWT; hydraulic power is taken as the control output, and the MPPT control strategy for HWT is proposed based on the feedback linearization control method. The strategy effectively solves the power tracking control problem and strong nonlinearity problem, and the system smoothly and quickly tracks the demand power. The efficiency is about 83%, which mainly depends on the mechanical efficiency and volumetric efficiency of the HWT key hydraulic components. Although the output power tracks the demand power, it fluctuates greatly. The main reason is that the proposed controller depends on the model parameters and includes the leakage coefficient and other time-varying parameters, which leads to poor real-time performance of the controller. However, the proposed theoretical controller provides a reference for practical applications. Therefore, based on the engineering requirements, the control law is simplified and verified by experiments; that is, the output power can track the demand power accurately and smoothly.

The impact of uncertainty and strong time-varying parameters of the HWT MPPT control will be further studied later.

Author Contributions: Data curation, L.C.; formal analysis, Y.Z., J.G. and Z.H.; funding acquisition, C.A.; validation, Q.H.; writing—original draft, W.G.; writing—review and editing, H.Q. All authors have read and agreed to the published version of the manuscript.

Funding: This research was funded by National Natural Science Foundation of China grant number [51775476] and funded by the Excellent Youth Project of Hebei grant number [E2018203388].

Conflicts of Interest: The authors declare no conflict of interest.

Nomenclature

Variable Symbol	Variable Specification
K_P	The optimal power coefficient, $K_P = \frac{\rho\pi R^5 C_{p\max}}{2\lambda_{opt}^3}$
P_{rmax}	Maximum wind power absorbed by the rotor
ρ	The air density
R	The radius of a rotor blade
v	The wind speed
$C_{p\max}$	The maximum coefficient of wind energy utilize
ω_{r}	The wind turbine speed
λ_{opt}	The optimum tip speed ratio
K_P	The maximum wind power coefficient
T_p	The pump torque
D_p	The pump displacement
p_h	The pressure difference between the pump suction and discharge lines
$\eta_{mech,p}$	The constant pump mechanical efficiency, which is assumed to be unity
$T_v\left(\omega_p, v\right)$	The rotor pneumatic torque
J_p	The pump moment of inertia
ω_p	The pump speed

B_p	The pump viscous damping coefficient
Q_p	The pump flow rate
C_{t1}	The pump leakage coefficient
T_m	The motor torque
D_m	The motor displacement
p_{h2}	The pressure difference between the motor suction and discharge lines
$\eta_{mech,m}$	The motor mechanical efficiency, which is assumed to be 1
K_m	The motor maximum displacement
γ	The motor swing angle, ranging from 0 to 1
T_L	The motor load torque
Q_{bl}	The proportional flow valve flow rate
K	The proportional coefficient
U_E	The voltage signal
Q_c	The flow rate caused by the oil compression.
V	The pressure-affected oil volume
β_e	The effective oil bulk modulus including a correction for hose expansion
J_m	The motor moment of inertia
ω_m	The motor speed
B_m	The motor viscous damping coefficient
Q_m	The motor flow rate
C_{t2}	The motor leakage coefficient
Q_{c1}	The compressibility flow between the pump and the flow control valve
Q_{c2}	The compressibility flow between the motor and the flow control valve
x_1	The state variable 1
x_2	The state variable 2
ω_{md}	The demand motor speed
z_1	The state variable after coordinate transformation 1
z_2	The state variable after coordinate transformation 2
e	The error
y_{d}	The system control input
y	The system control output
v^*	The system controller
k_1	The control parameter 1
k_2	The control parameter 2

References

1. Wei, J.; Sun, W.; Guo, A.; Wang, L. Analysis of wind turbine transmission system considering bearing clearance and thermo-mechanical coupling. In Proceedings of the World Non-Grid-Connected Wind Power Energy Conference, Nanjing, China, 24–26 September 2009; pp. 1–5.
2. Liu, Z.G.; Yang, G.L.; Wei, L.J.; Yue, D. Variable speed and constant frequency control of hydraulic wind turbine with energy storage system. *Adv. Mech. Eng.* **2017**, *9*, 1–10. [CrossRef]
3. Stelson, K.A. Saving the world's energy with fluid power. In Proceedings of the 8th JFPS Int. Symp. Fluid Power, Okinawa, Japan, 25–28 October 2011; pp. 1–7.
4. Jiang, Z.; Yang, L.; Gao, Z.; Moan, T. Numerical simulation of a wind turbine with a hydraulic transmission system. *Energy Procedia.* **2014**, *53*, 44–55. [CrossRef]
5. Pedersen, N.H.; Johansen, P.; Andersen, T.O. Optimal control of a wind turbine with digital fluid power transmission. *Nonlinear Dyn.* **2018**, *91*, 591–607. [CrossRef]
6. Yin, X.; Tong, X.; Zhao, X.; Karcanias, A. Maximum Power Generation Control of a Hybrid Wind Turbine Transmission System Based on H∞ Loop-Shaping Approach. *IEEE Trans. Sustain. Energy* **2019**. [CrossRef]
7. Ai, C.; Bai, W.; Zhang, T.; Kong, X. Research on the key problems of MPPT strategy based on active power control of hydraulic wind turbines. *J. Renew. Sustain. Energy* **2019**, *11*, 013301. [CrossRef]
8. Yin, X.; Zhao, X. Sensor-less Maximum Power Extraction Control of a Hydrostatic Tidal Turbine Based on Adaptive Extreme Learning Machine. *IEEE Trans. Sustain. Energy* **2019**, *11*, 426–435. [CrossRef]

9. Do, H.T.; Dang, T.D.; Truong, H.V.A.; Ahn, K.K. Maximum power point tracking and output power control on pressure coupling wind energy conversion system. *IEEE Trans. Ind. Electron.* **2018**, *65*, 1316–1324. [CrossRef]
10. Farbood, M.; Sha-Sadeghi, M.; Izadian, A.; Niknam, T. Advanced Model Predictive MPPT and Frequency Regulation in Interconnected Wind Turbine Drivetrains. In Proceedings of the 2018 IEEE Energy Conversion Congress and Exposition (ECCE), IEEE, Portland, OR, USA, 23–27 September 2018; pp. 3658–3663.
11. Li, S.; Shi, Y.; Li, J.; Cao, W. Maximum power point tracking control using combined predictive controller for a wind energy conversion system with permanent magnet synchronous generator. In Proceedings of the 2018 33rd Youth Academic Annual Conference of Chinese Association of Automation (YAC), IEEE, Nanjing, China, 18–20 May 2018; pp. 642–647.
12. Mulders, S.P.; Diepeveen, N.F.B.; van Wingerden, J.W. Extremum Seeking Control for optimization of a feed-forward Pelton turbine speed controller in a fixed-displacement hydraulic wind turbine concept. *J. Phys. Conf. Series. IOP Publ.* **2019**, *1222*, 012015. [CrossRef]
13. Deldar, M.; Izadian, A.; Anwar, S. A decentralized multivariable controller for hydrostatic wind turbine drivetrain. *Asian J.Control.* **2019**. [CrossRef]
14. Wang, F.; Chen, J.; Xu, B.; Stelson, K.A. Improving the reliability and energy production of large wind turbine with a digital hydrostatic drivetrain. *Appl. Energy* **2019**, *251*, 113309. [CrossRef]
15. Ai, C.; Wu, C.; Zhao, F.; Kong, X. Optimal power tracking control of a hydraulic wind turbine based on the active disturbance rejection control. *Trans. Can. Soc. Mech. Eng.* **2019**. [CrossRef]
16. Akbari, R.; Izadian, A.; Weissbach, R. An Approach in Torque Control of Hydraulic Wind Turbine Powertrains. In Proceedings of the 2019 IEEE Energy Conversion Congress and Exposition (ECCE), IEEE, Baltimore, MD, USA, 29 September–3 October 2019; pp. 979–982.
17. Wei, L.; Zhan, P.; Liu, Z.; Tao, Y.; Yue, D. Modeling and analysis of maximum power tracking of a 600 kw hydraulic energy storage wind turbine test rig. *Processes* **2019**, *7*, 706. [CrossRef]
18. Alberto, I. *Nonlinear Control Systems II*; Athenaeum Press Ltd.: Gateshead, UK, 1999.
19. Kong, X.D.; Ai, C.; Wang, J. A summary on the control system of hydrostatic drive train for wind turbines. *Chin. Hydraul. Pneum.* **2013**, *1*, 1–7.
20. Ai, C.; Chen, L.J.; Kong, X.D. Characteristics simulation for hydraulic wind turbine. *China Mach. Eng.* **2015**, *26*, 1527–1531.
21. Jiang, Z.H.; Yu, X.W. Modeling and control of an integrated wind power generation and energy storage system. In Proceedings of the Power Energy Soc. General Meeting, Calgary, AB, Canada, 26–30 July 2009; pp. 1–8.
22. Wang, J.H. *Advanced Nonlinear Control Theory and Its Application*; Beijing Science Press: Beijing, China, 2012.
23. Sreenath, K.; Park, H.W.; Poulakakis, I.; Grizzle, J.W. A compliant hybrid zero dynamics controller for stable, efficient and fast bipedal walking on MABEL. *Int. J. Rob. Res.* **2011**, *30*, 1170–1193. [CrossRef]
24. Bharadwaj, S.; Rao, A.V.; Kenneth, D.M. Entry trajectory tracking law via feed-back linearization. *J. Guid. Control Dyn.* **1998**, *21*, 726–732. [CrossRef]